Detailed seafloor imagery of turbidity current bedforms reveals new insight into fine-scale near-bed processes

Alexandre Normandeau, Patrick Lajeunesse, Jean-françois Ghienne, Pierre Dietrich

Detailed Seafloor Imagery of Turbidity Current Bedforms Reveals New Insight Into Fine-Scale Near-Bed Processes

Alexandre Normandeau[1] [ORCID], **Patrick Lajeunesse[2]** [ORCID], **Jean-François Ghienne[3]**, and **Pierre Dietrich[4]**

[1]Geological Survey of Canada (Atlantic), Natural Resources Canada, Dartmouth, NS, Canada, [2]Département de Géographie, Université Laval, Québec, QC, Canada, [3]Institut de Physique du Globe de Strasbourg, UMR 7516 CNRS/Université de Strasbourg, Strasbourg, France, [4]Géosciences Rennes, UMR6118, Université de Rennes 1, Rennes, France

Abstract High-resolution imagery of the morphological character of modern active turbidite systems are critical for understanding the complexity of turbidity current processes occurring on the seafloor. Here, we describe a 30 cm-resolution autonomous underwater vehicle repeat bathymetric dataset that allows to significantly increase the geomorphological detail of crescentic bedforms in turbidite systems. This repeat imagery shows the erosion produced by dense basal layers at the base of turbidity currents, the inception of plunge pools, and the controls that hydraulic jump troughs have on subsequent flow path of weaker turbidity currents. Transverse small-scale scours located in cyclic step troughs suggest that weak flows follow local relief, therefore explaining the wide variability of turbidity current flow indicators observed in outcrops. This imagery demonstrates that turbidite systems are formed by the superimposition of erosion surfaces and depositional patterns recording contrasted flow behavior and provides new views on turbidity current behavior in natural environments.

Plain Language Summary Turbidity currents transport large amounts of sediment, macro-nutrients and carbon to the deep-sea. During their passage, they generate a wide variety of bedforms, from which these flows can be reconstructed. However, the lack of detailed and very high-resolution imagery of these bedforms prevents detailed understanding of the 3D behavior of turbidity currents. In this paper, we describe a 30 cm-resolution autonomous underwater vehicle repeat bathymetric dataset that allows to map very-fine scale features of turbidity current bedforms. This repeat imagery reveals the erosion produced by the base of turbidity currents and shows the formation of new small-scale scours linked to the currents. The data also reveals the effect of large turbidity currents on the subsequent path of smaller ones. This high-resolution imagery allows to bridge the gap between observations on the modern seafloor and those observed in outcrops.

1. Introduction

Turbidity currents are important conveyors of sediment, macro-nutrients and carbon to the deep-sea (Mignard et al., 2017; Pirmez & Imran, 2003). During their passage, they generate a wide variety of bedforms such as dunes, antidunes and cyclic steps (Kostic, 2011). Turbidity current flow reconstructions are made from the deposits and bedforms they leave behind (Cartigny et al., 2011; Kostic, 2011). Generally, morphological parameters such as wavelength, wave height and slope are used for the reconstruction of flow conditions (Cartigny et al., 2011; Hand, 1974; Kostic, 2011; Normandeau et al., 2019). However, these flow reconstructions assume that bedforms are essentially 2D features, in which turbidity current flows are unidirectional and in full equilibrium with the seabed topography. In reality, turbidity currents probably flow in a much more complex manner, as it has long been recognized that flow direction indicators in outcrops vary with a standard deviation of 30° (Glennie, 1963; Kuenen, 1957). For example, the local effect of hydraulic jumps, sediment cohesion and inherited bedforms are susceptible to play a major role in sediment remobilization, deposition and flow direction through time, which may affect sedimentary structures and facies observed in the sedimentary record (Eggenhuisen et al., 2010; Ghienne et al., 2021). Conversely, some structures shaped during a turbidity current event might not be preserved in the sedimentary record due to subsequent erosion. Therefore, high-resolution images of modern active turbidite systems are critical for increasing the inventory of turbidity current bedforms and understanding the complexity of turbidity current processes occurring on the seafloor.

For the last three decades, multibeam echosounders (MBES) have allowed marine geologists to map turbidity current bedforms (e.g., Smith et al., 2007). However, there is still a large discrepancy between the morphologies

that can be observed on the modern seafloor (usually 10–100 m-scale) and the small-scale bedforms and structures observed in outcrops (cm-to m-scale). The advent of autonomous underwater vehicles (AUV) that can navigate near the seafloor using higher frequency MBES now allow filling this scale gap by producing higher resolution bathymetric imaging of the seafloor to image smaller-scale (≤1 m) bedforms and structures (Fildani et al., 2021; Maier et al., 2012, 2011; C. K. Paull et al., 2013).

Multibeam bathymetry data collected over the Pointe-des-Monts turbidity current system since 2007 revealed the presence of upslope migrating crescentic bedforms (λ = 30–60 m, h = 1–3 m) and sediment waves, outlining that they are linked to cyclic step instabilities (Normandeau et al., 2014, 2020). Subsequent repeat bathymetry and Acoustic Doppler Current Profiler (ADCP) mooring showed that turbidity currents are triggered during storms (Normandeau et al., 2020). Some of the recorded flows were slow-moving ($u \leq 0.5$ m s^{-1}) and dilute and did not lead to the migration of the bedforms. However, during stronger events where $u > 0.5$ m s^{-1}, crescentic bedforms migrated upslope in the channelized region, producing lee-side erosion and stoss-side deposition along trains of cyclic steps. AUV surveys conducted in 2019 and 2020 off Pointe-des-Monts, in the St. Lawrence Estuary (eastern Canada; Figure 1a), allowed mapping the seafloor at a 30 cm horizontal resolution over a field of active turbidity current bedforms (Normandeau et al., 2014, 2020). In this paper, we present the results of these surveys that reveal detailed seafloor morphologies produced by the passage of turbidity currents. These surveys allow imaging in detail the variability in turbidity current flow paths and their effect on bedform morphologies and the thickness of the eroding dense basal layers of turbidity currents.

2. Methods

The Pointe-des-Monts canyon/channel system is a well-documented active system (Normandeau et al., 2014, 2020) which has been surveyed with a hull-mounted EM-2040 in 2012, 2015, 2016, 2017, 2018, and 2019; the data up to 2017 was recently reported in Normandeau et al. (2020). Here we present the results of two AUV surveys completed in 2019 and 2020 and compare them to a 2018 hull-mounted survey. Three dives were conducted with an AUV in May 2019 and October 2020 at 30 m above the bottom of the submarine canyons using a Kongsberg Hugin (Figure 1a and Figures S1–S2 in Supporting Information S1) equipped with a 400 kHz Kongsberg EM-2040. The 1° × 1° beamwidth and up to 800 soundings per pings allowed the data to be gridded at 30 cm horizontal resolution. The vertical resolution is ∼1 cm, allowing to image the fine scale details of the seafloor down to a depth of 300 m. Sub-bottom profiler data was also collected using the Hugin Edgetech 3100 2–16 kHz Chirp.

A hydrological analysis of the AUV data allowed imaging flow pathways. This hydrological analysis consisted of filling the basins in the digital elevation model (DEM). The filling of the basins in the DEM allowed identifying pools and their depths. Pools smaller than 2 m^2 were removed from the visualisations because many of them were due to noise in the bathymetric data. Flow direction and flow accumulation rasters were then created with the filled surface to illustrate the hydrologic connectivity of the canyon/channel floor and related first and second-order structures.

3. Results

3.1. 2018–2019 Bedform Migration From Hull-Mounted MBES Surveys

The 2019 hull-mounted survey allows comparing the morphology of the canyons with the previous 2018 hull-mounted survey. A difference in elevation map shows that migration of the crescentic bedforms occurred though the main canyon/channel system, indicating that it was affected by turbidity currents. In the main canyon/channel, up to ∼30 m of upslope migration was observed between the 2 years, with stronger migration rates in the narrow part of the canyon where the four upslope reaches merge (Figures 1a and 1b). Upslope migration of bedforms occurred in the three eastern reaches whereas the western one does not show evidence of bedform migration. Upslope migration of bedforms extended to a depth of ∼250 m (Figures 1a and 1b).
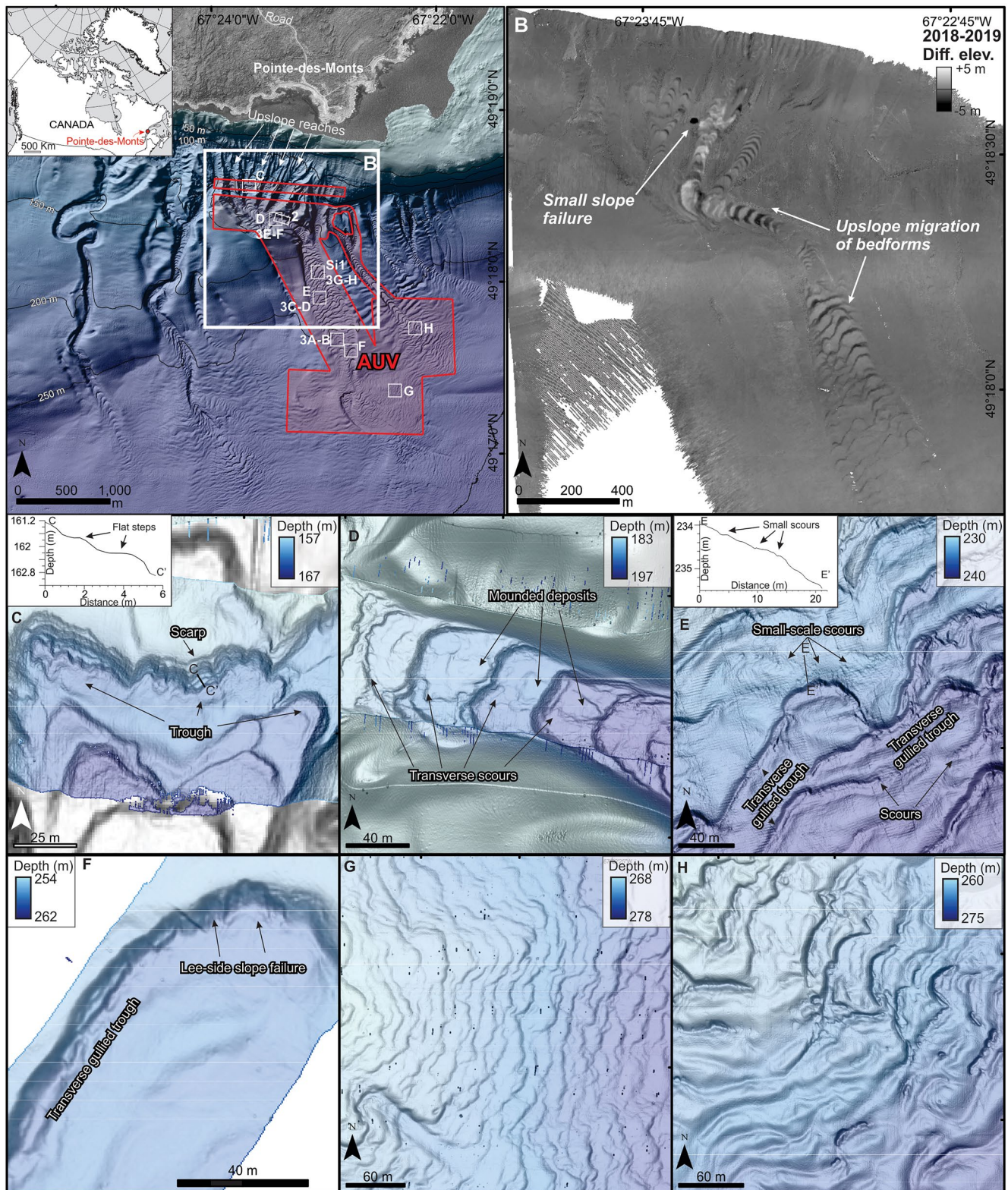
Figure 1. The turbidite system of Pointe-des-Monts, Lower St. Lawrence Estuary, eastern Canada. (a) Location of the 2019 AUV survey of the canyon/channel system. (b) Difference maps between 2018 and 2019 illustrating the upslope migration of crescentic bedforms. (c) High-resolution swath bathymetry imagery (0.3 m horizontal resolution) of crescentic bedforms with a stepped lee-side (2019). (d) Crescentic bedforms with transverse scours and mounded deposits (2019). (e) Crescentic bedforms with small-scale scours overprinting the larger bedforms (2019). (f) Erosional slope failures on the lee side of a bedform (2020). (g) Small-scale bedforms on the fan (2019). (h) Crescentic bedforms evolving on the fan (2019).

3.2. AUV Observation of the 2019 Turbidity Current Bedforms

3.2.1. Upper Reach

In the upper reaches of the main canyon, the crescentic bedforms are mostly 30–50 m-long and generally characterized by a smooth stoss side (Figure 1c). The stoss side consists of a gentle reverse slope that begins with a deep (∼1 m) and wide (≤20 m) pool in the trough. The trough-to-stoss transition is generally clearly expressed by a short (∼5 m) and steeper (5–15°) reverse slope. The steep (up to 24°) lee sides are either smooth or stepped. The stepped appearance is characterized by small-scale scarps at the crest of the bedforms followed downslope by nearly flat steps <1.5 m wide (Figure 1c).

3.2.2. Mid Reach

Where the four upper reaches merge into one canyon (Figure 1a), the morphological appearance of the bedforms becomes much more complex (Figure 1d). A steep erosional wall separates the crescentic bedforms from the smooth canyon wall, suggesting that the crescentic bedforms interact with the canyon walls only in the bottom 3 m (Figures 2b–2d). The erosional wall is higher adjacent to the trough of the bedforms and thins toward its crests (Figures 2d and 2e). The crests also become more sinuous while remaining overall crescentic (Figure 2b). The crests frequently show ∼5 m-wide, juxtaposed, small-scale scours within the larger crescentic bedforms (Figure 2b). In the narrowest part of the canyon, the lee side becomes smoothly linear, without visible steps. In addition, the pools in the troughs are much shallower than those located upstream (30 cm-deep at most) and narrower (∼6 m-large). Although the pools are shallower and narrower, they have a more chaotic appearance with the presence of second-order, 0.4 m-high, transverse crescentic scours oriented perpendicular to the canyon direction and parallel to the lee sides (Figure 1d). The perpendicular-to-canyon scours run downslope along the first-order bedform troughs before bifurcating back down-canyon, which is well illustrated by the hydrological analysis of the DEM (Figure 2c). On the stoss side, erosional and depositional features are chaotic due to these transverse scours. Mounded deposits are surrounded by steeper slopes and smaller scarps (Figure 2b).

3.2.3. Lower Reach

Where the channel becomes less confined downslope, bedform morphology remains complex. In numerous places, the stoss side is rugged, scattered with small scale scours less than 0.1 m-high and 2 m-wide (Figure 1e). In the troughs, 2 m-wide and 0.2 m-deep pools are present. In some of them, small scarps run perpendicular to channel orientation, creating transverse gully like morphology in the trough (Figures 1e and 1f). On some of the crests, the reverse slope of the stoss sides increases in the last 2–3 m before the lee side, increasing the slope by as much as ∼5–6° (Figures 3g–3s-3) and defining an unexpected narrow and sharp crest. These incease in slope angles at the crest are observed only on oblique crests downslope (S-3). Farther downslope, second-order scours (5 m-wide, 1 m-high) are present above and on the lee slopes (Figures 1e and 1f).

3.2.4. Unconfined Submarine Fan

Where the channel becomes unconfined downslope, the morphology of the bedforms changes considerably from a crescentic to a sinuous aspect (Figure 1g). Where channel unconfinement is abrupt, such as on the eastern gullies, crescentic bedforms continue on the lobe for a few hundred meters (Figure 1h). Longer-wavelength bedforms (60–100 m-long, 1–2 m-high) are present on each side of the crescentic bedforms. They are linear to sinuous, with similar stoss and lee length but showing lee slopes steeper (∼4°) than stoss slopes (1.5°). Where the crescentic bedforms dissipate, they are replaced with sinuous bedforms (Figures 1g and 1h) which are 20–30 m-long and 0.2–0.4 m-high.

3.3. Comparison Between 2019 and 2020 AUV Observations of Crescentic Bedforms

A second AUV survey of the main canyon/channel floor was completed in 2020 and shows that turbidity currents occurred between 2019 and 2020 as evidenced by crescentic bedforms that migrated upstream (Figure 3). Positioning errors due to navigation issues prevent us from quantifying precisely the upstream migration, which is estimated 5–10 m in average; however, it allows to qualitatively examine the fine-scale changes on the seabed. A notable difference between the datasets is the smoothness of the bedforms in the mid-reach compared to 2019. In 2020, second-order, perpendicular-to-axis scours characterizing the 2019 mid-reach channels are no longer present. The channel rather displays typical smoothed bedforms (Figures 3e and 3f).
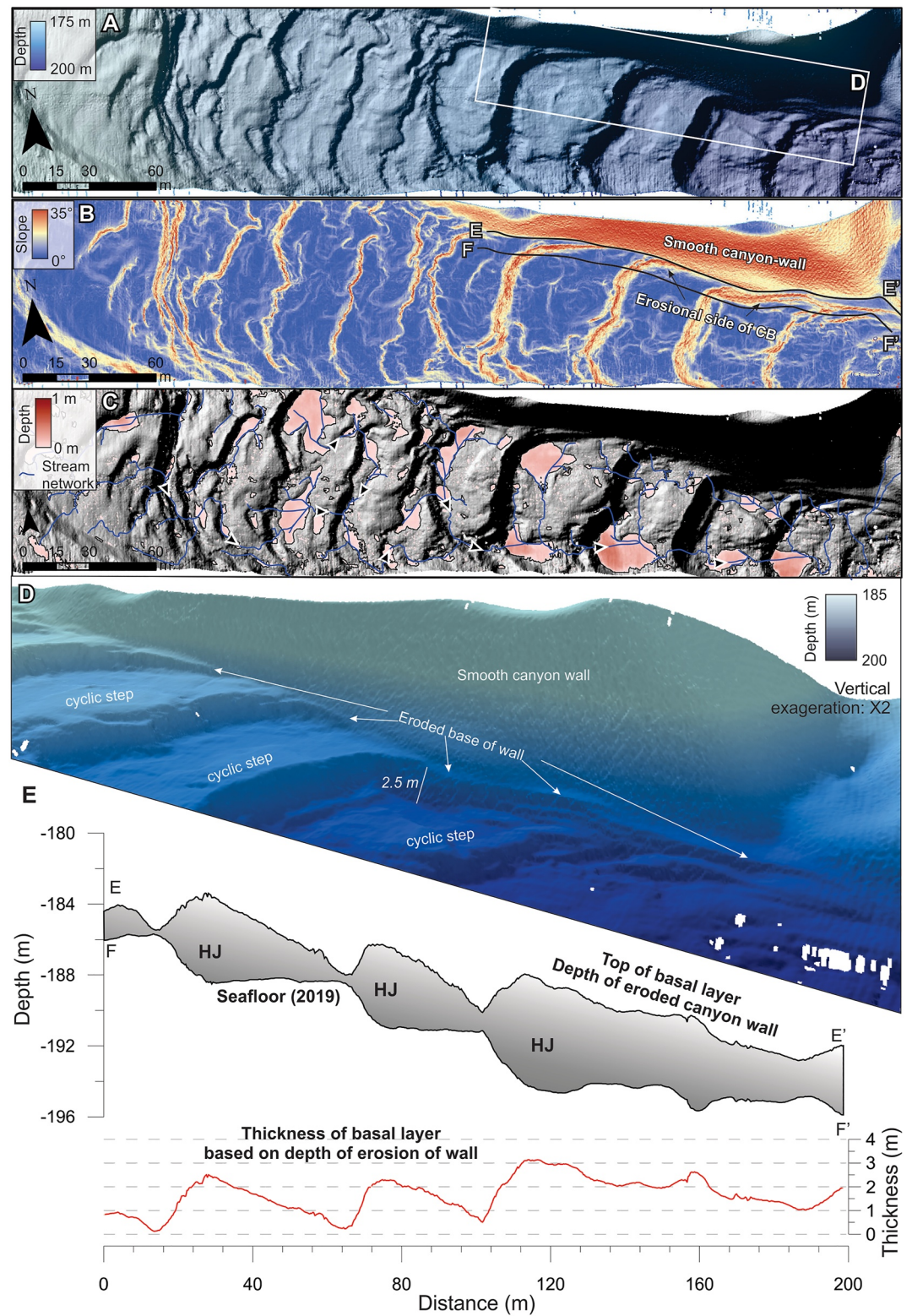
Figure 2. (a) AUV MBES of the main canyon. (b) Slope map of the main canyon. (c) Hydrological analysis illustrating the formation of closed depressions (pools) along with stream network when the depressions are filled illustrating the most likely pathway of downslope currents. (d) 3D view of the erosion at the base of the canyon wall. (e) Profiles of bedforms (F–F') and of the top of the eroded part of the canyon wall (E–E') illustrating the thickness of the erosive dense basal layer in a turbidity current.
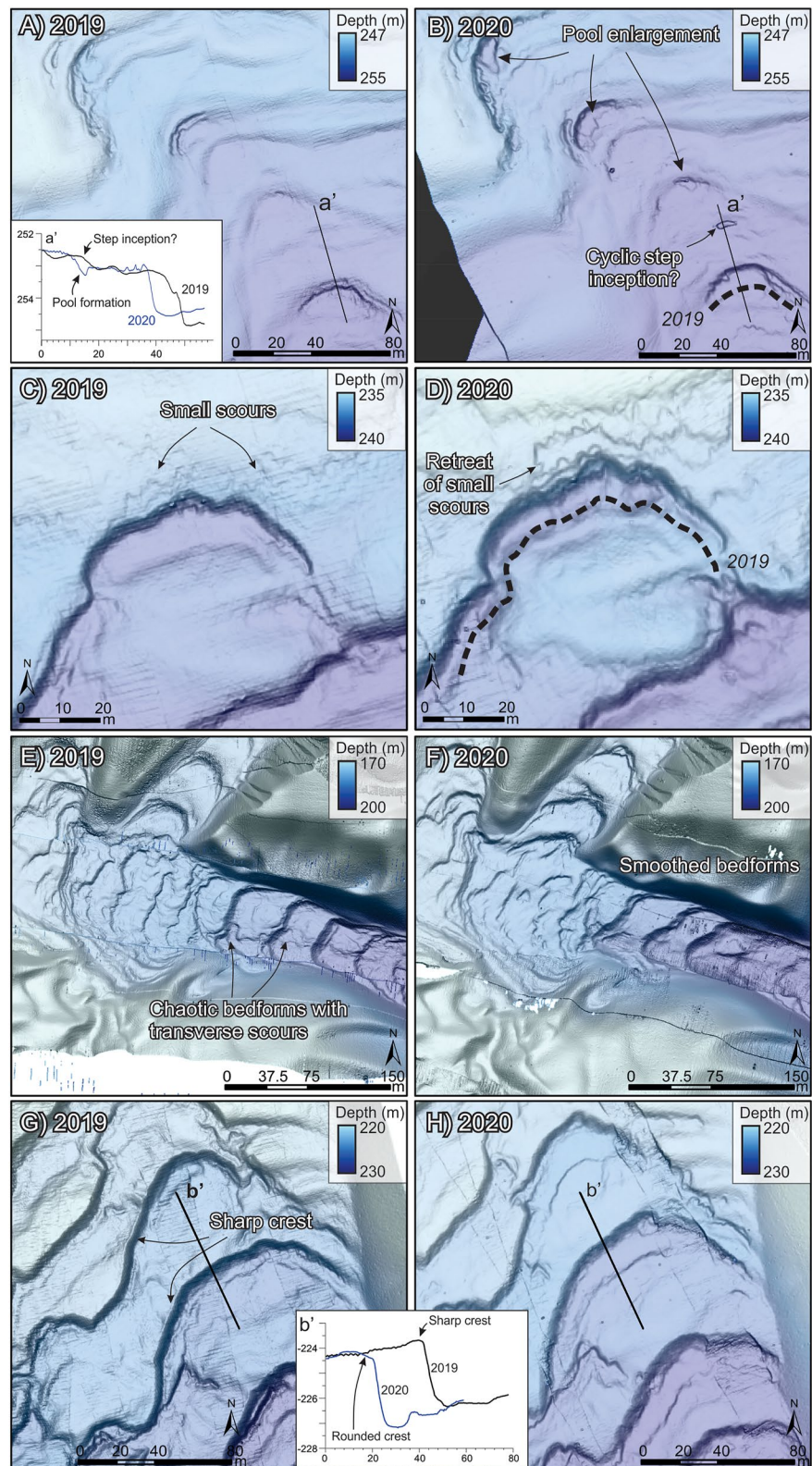
Figure 3. 2019 versus. 2020 survey over specific locations in the Pointe-des-Monts system. (a and b) inception of a cyclic step between the two surveys and the enlargement of pools. (c and d) upslope migration of cyclic steps (first order bedform) and of small scours at the crest (second order bedforms). (e and f) Smoothing of the bedforms in the main canyon area between the two surveys, (g and h) Sharp crested crest in 2019 rounded in 2020 illustrated in b' profile.

The 2020 survey also shows the formation and enlargement of pools (Figures 3a and 3b). In 2019, Figure 3a shows smooth crescentic bedforms. In 2020, a small-scale 50 cm-deep crescentic scour was formed 30 m upslope from one of the bedform and many of the other pools were enlarged. Similar small scours are present at the crest of many of the crescentic bedforms in the lower channel (Figures 3c and 3d). These small scours are present both in 2019 and 2020 where they form a stepped pattern on the crest to lee side of the bedforms, but they have migrated upstream. Last, the narrow ridges at the crest of lower reach bedforms (sharp crests in Figure 3g) are no longer visible in 2020 (Figures 3g and 3h). However, the gullied troughs remained visible (Figures 3g and 3h)

4. Discussion

4.1. How Erosive Are Turbidity Currents?

Crescentic bedforms such as those observed in the channel thalweg have been interpreted as cyclic steps at Pointe-des-Monts (Normandeau et al., 2020) and elsewhere (Hage et al., 2018; Hughes Clarke, 2016). Cyclic step bedforms are bounded by hydraulic jumps and are characterized by thin and fast supercritical flows on the lee side and slow and thick subcritical flows on the stoss side. Cyclic steps instabilities such as those are believed to be formed under stratified flows (Hughes Clarke, 2016; Postma & Cartigny, 2014). The AUV MBES mapping at Pointe-des-Monts supports this hypothesis since it shows that erosion of canyon walls occurs only in the bottom 3 m of the canyon (Figure 2). This near-bed erosion illustrates the erosive nature of the basal part of a turbidity current as expected in stratified flows and suggests that the dense basal layer is the driving force of seabed changes in turbidity currents (Hughes Clarke, 2016; C. K. Paull et al., 2018).

On the lower reach of the system, inception of a crescentic bedform, through the formation of a plunge pool, is clearly observed by the erosion and amplification of a small scour (Figures 3a and 3b). These small scours are probably formed by hydraulic jumps in an overriding turbidity currents, which is created due to internal flow properties (Guiastrennec-faugas et al., 2020; Heijnen et al., 2020) and to pre-existing defects on the seabed. These scours are enlarged by subsequent flows and eventually create a crescentic bedform of their own or are caught up by another upstream migrating bedform. Such second-order, small 1–5 m-long scours and cyclic steps have been identified in outcrop studies (Cornard & Pickering, 2019; Ghienne et al., 2021) but were yet to be identified in modern seafloor systems.

4.2. Variability in Flow Paths of Turbidity Currents

The two AUV surveys completed at Pointe-des-Monts show first-order bedforms (20–60 m long crescentic bedforms) and second-order morphologies (≤5 m long bedforms and scours, and transverse gullies) that developed superimposed on the first-order bedforms. The first-order bedforms correspond to the development of cyclic steps instabilities, which allows the overall upstream migration of the crescentic bedforms. The second-order morphology is believed to be attributed to smaller, dilute flows that may correspond to the tail-end of vigorous turbidity currents or may be triggered during separate, less energetic events.

Eggenhuisen et al. (2010) suggested that interaction of the base of the flow with small-scale scours affects flow direction up to 15°. Here we show that small scours and other second-order bedforms are in some cases oriented 90° from channel direction, creating transverse gullies in the trough of bedforms. These transverse turbidity currents appear to be due to the formation of hydraulic jumps in troughs; during large turbidity current events, deep (1–3 m) pools are formed at the lee-to-stoss transition that favors a rapid flow deceleration and generates this hydraulic jump (Figure 4a). These deep pools in turn create a confined space where subsequent flows are partly trapped (Figure 4b). When subsequent small turbidity currents travel in the troughs, their flow path is believed to be forced to follow local relief which might be perpendicular to the main canyon orientation (Figures 2d and 4b). By doing so, they create their own smaller transverse scours and gullies on their path. These small-scale turbidity currents could either correspond to the tail-end of large flows or more dilute flows incapable of leading to the upslope migration of the larger bedforms. In 2017, both types of turbidity currents were observed at Pointe-des-Monts (Normandeau et al., 2020): one that led to significant changes on the seabed and another that was characterized by weaker velocities and that only produced minor changes of the seabed. It is unlikely that the main part of the larger flows would create those perpendicular flows since observation both at Pointe-des-Monts and elsewhere have shown that dense basal layers are present during the faster sections of the flows. The dense basal layers probably wipe out small-scale bedforms but would be responsible for the creation of the deep
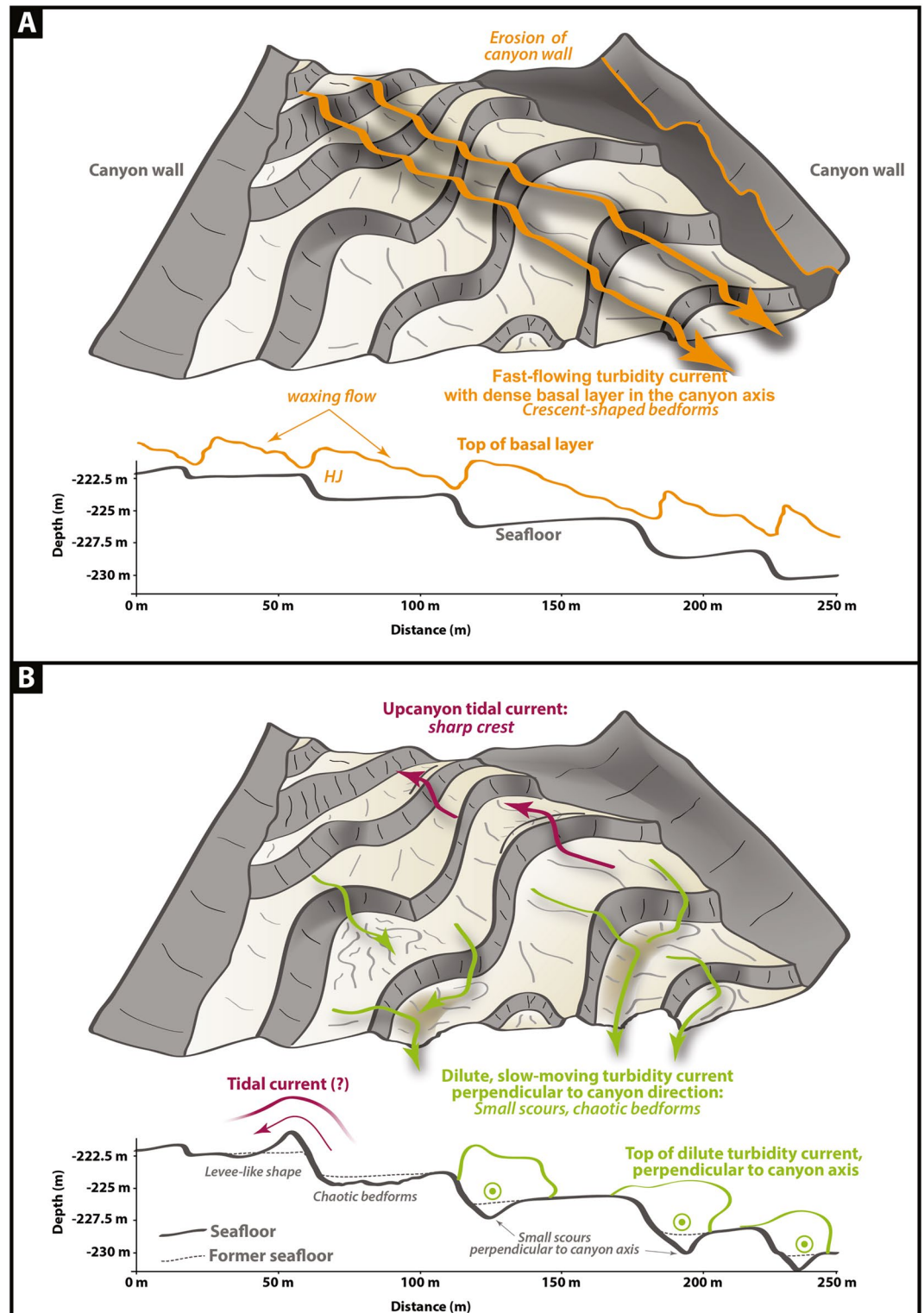
Figure 4. Conceptual model of 1st order (a) and second-order bedforms (b) on a cyclic step system. (a) Cyclic step events leads to 1st order modification of the seabed whereas (b) small and dilute turbidity current follows the bathymetry created by (a) and forms transverse gullies and scours. In addition, tidal currents reshape the crest of bedforms.

troughs. Large flows between 2019 and 2020 are probably responsible for wiping out the transverse scours in the main narrow channel (Figure 3f). These flow types running perpendicular to the main flow direction have not been observed in flume tank experiments, probably due to the confined nature of the flows created in laboratory and the short-lasting time of the tail of turbidity currents, which can last hours to weeks in natural flows (e.g., Azpiroz-Zabala et al., 2017).

4.3. Preservation of First-Order and Second-Order Bedforms

Although there is an overall preservation of first-order bedforms through their upstream migration, many of the second-order bedforms (i.e., small transverse scours and sharp and narrow crests) present on the 2019 survey are either absent or have been smoothed on the 2020 AUV survey. The smoothing of second-order bedforms on 2020 AUV survey suggests that the last event to have occurred on the system prior to the survey is a high-energy one that mainly led to the migration of cyclic steps. Ghienne et al. (2021) indicated that the cyclic step depositional record is dominated by cyclic step stratal architecture which encompass a significant proportion of sedimentary deposits not related to cyclic step flow events. These authors suggested that deposition originated from a complex succession of (a) high-energy turbidity currents that left behind cyclic step morphologies and (b) low-energy events that partly remodeled pre-existing cyclic step morphologies, but whose original bedform morphology were not preserved. Therefore, a large swath of transportation/depositional processes is downplayed in modern turbidity current studies whilst their stratigraphic expression locally constitutes an important part of the depositional record. Our AUV imagery further suggests that many flows in channel showing cyclic step morphologies do not actually develop a cyclic-step instability but rather form second-order bedforms, which are probably buried on the stoss side of the bedforms during subsequent flows.

Second-order bedforms, which are not preserved in the 2020 survey, also appear to have been formed during quiet conditions by tidal currents. A unique feature of the high-resolution imagery collected in 2019 is the presence of narrow and sharp crests on bedforms running oblique to the channel direction (Figure 3g). These sharp-crested features are similar to what is observed on the crest of eolian dunes (Jackson et al., 2020; Yuxiang et al., 2017). Wind can form sharp-crested dunes, which are then rounded during wind-reversal. In marine settings, tidal currents could act similarly to wind over eolian dunes: during ebb conditions, the downcanyon flow focuses sediments at the crest of the bedforms. These sharp crests are present in 2019 but absent in 2020, suggesting the passage of a strong turbidity current that wiped out those types of features (Figure 3h) or possibly that an up-canyon tidal current rounded the crest of the bedforms. Our findings therefore indicate that deposits originating from tidal currents might locally be observed in (fossil) turbidite systems.

Some of the second-order features preserved in the stratigraphic record are the small-scale scours and stepped profile of the lee side of the crescentic bedforms (Ghienne et al., 2021). Experimental studies have shown that these erosional scours and stepped profile on knickpoint can be due to erosion by turbidity currents or a landsliding process on the knickpoint headscarp (Turmel et al., 2012). In their experiment, Turmel et al. (2012) observed that knickpoint migration could also occur without an overriding turbidity currents, indicating that both hydraulic and geotechnical properties of sediments need to be considered for understanding their evolution. Therefore, the many small scours on the lee side of the crescentic bedforms (Figure 1f) cannot necessarily be attributed to a turbidity current. When subsequent turbidity current fill in these features, these erosional scours can be preserved in the stratigraphic record (Cornard & Pickering, 2019; Ghienne et al., 2021).

5. Conclusions

The 30-cm horizontal resolution AUV MBES imagery reported in this paper presents a significantly different view of crescentic bedforms occurring in turbidity current systems than previously possible using conventional hull-mounted MBES. This fine-scale morphological analysis is an essential step in understanding the complex 3D and time-averaged behavior of turbidity currents and related deposits in natural environments. These new seafloor images show that first-order and second-order bedforms and morphologies co-exists momentarily on the seafloor. For example, bedform troughs formed by hydraulic jumps in cyclic steps control subsequent flow path of weaker turbidity currents. These weaker turbidity currents then form transverse gullies and scours, which have been smoothed out on the repeated AUV survey completed in this study. Such a suite of processes can explain the wide variability of turbidity current flow indicators observed in outcrops. First-order bedforms such as cyclic

step and sediment waves are mostly preserved from one survey to the other, although they migrated upslope. On the other end, second-order bedforms such as transverse scours and gullies and lee-side failures are wiped-out, remodeled or buried by subsequent flows over time.

High-resolution imaging of the complex morphology of crescentic bedforms and sediment waves provide new perspectives on how turbidity currents behave and how related bedforms evolve through time in natural environments; processes that were not possible to document in modern systems due to lower-resolution observations using conventional seafloor mapping systems. We emphasize that the 3D approach to interpreting outcrops is critical in order to fully understand past flow variability over one particular turbidite system.

Data Availability Statement

The AUV data presented in this paper are available on the St. Lawrence Global Observatory website: https://doi.org/10.26071/ogsl-a877175e-33cc.

References

Azpiroz-Zabala, M., Cartigny, M. J. B., Talling, P. J., Parsons, D. R., Sumner, E. J., Clare, M. A., et al. (2017). Newly recognized turbidity current structure can explain prolonged flushing of submarine canyons. *Science Advances*, *3*(10), e1700200. https://doi.org/10.1126/sciadv.1700200

Cartigny, M. J. B., Postma, G., Van Den Berg, J. H., & Mastbergen, D. R. (2011). A comparative study of sediment waves and cyclic steps based on geometries, internal structures and numerical modeling. *Marine Geology*, *280*(1–4), 40–56. https://doi.org/10.1016/j.margeo.2010.11.006

Cornard, P. H., & Pickering, K. T. (2019). Supercritical-flow deposits and their distribution in a submarine channel system, Middle Eocene, Ainsa Basin, Spanish Pyrenees. *Journal of Sedimentary Research*, *89*(6), 576–597. https://doi.org/10.2110/jsr.2019.34

Eggenhuisen, J. T., Caffrey, W. D. M. C., Haughton, P. D. W., & Butler, R. W. H. (2010). Small-scale variability in turbidity-current flow controlled controlled by roughness resulting from substrate erosion: Field evidence for a feedback mechanism. *Journal of Sedimentary Research*, *80*, 129–136. https://doi.org/10.2110/jsr.2010.014

Fildani, A., Kostic, S., Covault, J. A., Maier, K. L., Caress, D. W., & Paull, C. K. (2021). Exploring a new breadth of cyclic steps on distal submarine fans. *Sedimentology*, *68*(4), 1378–1399. https://doi.org/10.1111/sed.12803

Ghienne, J., Normandeau, A., Dietrich, P., Bouysson, M., Lajeunesse, P., & Schuster, M. (2021). The depositional signature of cyclic steps: A late quaternary analogue compared to modern active delta slopes. *Sedimentology*, *68*(4), 1502–1538. https://doi.org/10.1111/sed.12806

Glennie, K. W. (1963). An interpretation of turbidites whose sole markings show multiple directional trends. *The Journal of Geology*, *71*(4), 525–527. https://doi.org/10.1086/626924

Guiastrennec-faugas, L., Gillet, H., Peakall, J., Dennielou, B., Gaillot, A., & Jacinto, R. S. (2020). Initiation and evolution of knickpoints and their role in cut-and-fill processes in active submarine channels. *Geology*, *49*, 1–6. https://doi.org/10.1130/G48369.1/5177786/g48369.pdf

Hage, S., Cartigny, M. J. B., Clare, M. A., Sumner, E. J., Vendettuoli, D., Clarke, J. E. H., et al. (2018). How to recognize crescentic bedforms formed by supercritical turbidity currents in the geologic record: Insights from active submarine channels. *Geology*, *46*(6), 563–566. https://doi.org/10.1130/g40095.1

Hand, B. M. (1974). Supercritical flow in density currents. *Journal of Sedimentary Petrology*, *44*(3), 637–648.

Heijnen, M. S., Clare, M. A., Cartigny, M. J. B., Talling, P. J., Hage, S., Lintern, D. G., et al. (2020). Rapidly-migrating and internally-generated knickpoints can control submarine channel evolution. *Nature Communications*, *11*(1), 1–15. https://doi.org/10.1038/s41467-020-16861-x

Hughes Clarke, J. E. (2016). First wide-angle view of channelized turbidity currents links migrating cyclic steps to flow characteristics. *Nature Communications*, *7*, 11896. https://doi.org/10.1038/ncomms11896

Jackson, D. W. T., Cooper, A., Green, A., Beyers, M., Guisado-pintado, E., Wiles, E., et al. (2020). Reversing transverse dunes: Modelling of airflow switching using 3D computational fluid dynamics. *Earth and Planetary Science Letters*, *544*, 116363. https://doi.org/10.1016/j.epsl.2020.116363

Kostic, S. (2011). Modeling of submarine cyclic steps: Controls on their formation, migration, and architecture. *Geosphere*, *7*(2), 294–304. https://doi.org/10.1130/ges00601.1

Kuenen, P. H. (1957). Sole markings of graded graywacke beds. *The Journal of Geology*, *65*(3), 231–258. https://doi.org/10.1086/626429

Maier, K. L., Fildani, A., McHargue, T. R., Paull, C. K., Graham, S. a., & Caress, D. W. (2012). Punctuated deep-water channel migration: High-resolution subsurface data from the Lucia Chica channel system, offshore California, U.S.A. *Journal of Sedimentary Research*, *82*(1), 1–8. https://doi.org/10.2110/jsr.2012.10

Maier, K. L., Fildani, A., Paull, C. K., Graham, S. A., McHargue, T. R., Caress, D. W., & McGann, M. (2011). The elusive character of discontinuous deep-water channels: New insights from Lucia Chica channel system, offshore California. *Geology*, *39*(4), 327–330. https://doi.org/10.1130/g31589.1

Mignard, S. L.-A., Mulder, T., Martinez, P., Charlier, K., Rossignol, L., & Garlan, T. (2017). Deep-sea terrigenous organic carbon transfer and accumulation: Impact of sea-level variations and sedimentation processes off the Ogooue River (Gabon). *Marine and Petroleum Geology*, *85*, 35–53. https://doi.org/10.1016/j.marpetgeo.2017.04.009

Normandeau, A., Bourgault, D., Neumeier, U., Lajeunesse, P., St-Onge, G., Gostiaux, L., & Chavanne, C. (2020). Storm-induced turbidity currents on a sediment-starved shelf: Insight from direct monitoring and repeat seabed mapping of upslope migrating bedforms. *Sedimentology*, *67*, 1045–1068. https://doi.org/10.1111/sed.12673

Normandeau, A., Campbell, D. C., & Cartigny, M. J. B. (2019). The influence of turbidity currents and contour currents on the distribution of deep-water sediment waves offshore eastern Canada. *Sedimentology*, *66*(5). https://doi.org/10.1111/sed.12557

Normandeau, A., Lajeunesse, P., St-Onge, G., Bourgault, D., Drouin, S. S. O., Senneville, S., & Bélanger, S. (2014). Morphodynamics in sediment-starved inner-shelf submarine canyons (Lower St. Lawrence Estuary, Eastern Canada). *Marine Geology*, *357*, 243–255. https://doi.org/10.1016/j.margeo.2014.08.012

Paull, C. K., Caress, D. W., Lundsten, E., Gwiazda, R., Anderson, K., McGann, M., et al. (2013). Anatomy of the La Jolla Submarine Canyon system; offshore southern California. *Marine Geology*, *335*, 16–34. https://doi.org/10.1016/j.margeo.2012.10.003

Paull, C. K., Talling, P. J., Maier, K. L., Parsons, D., Xu, J., Caress, D. W., et al. (2018). Powerful turbidity currents driven by dense basal layers. *Nature Communications*, *9*, 1–9. https://doi.org/10.1038/s41467-018-06254-6

Pirmez, C., & Imran, J. (2003). Reconstruction of turbidity currents in Amazon Channel. *Marine and Petroleum Geology*, *20*(6–8), 823–849. https://doi.org/10.1016/j.marpetgeo.2003.03.005

Postma, G., & Cartigny, M. J. B. (2014). Supercritical and subcritical turbidity currents and their deposits—A synthesis. *Geology*, *42*(11), 987–990. https://doi.org/10.1130/g35957.1

Smith, D. P., Kvitek, R., Iampietro, P. J., & Wong, K. (2007). Twenty-nine months of geomorphic change in upper Monterey Canyon (2002–2005). *Marine Geology*, *236*(1–2), 79–94. https://doi.org/10.1016/j.margeo.2006.09.024

Turmel, D., Locat, J., & Parker, G. (2012). Upstream Migration of Knickpoints: Geotechnical Considerations. In Y. Yamada (Ed.), *Submarine mass movements and their consequences*, *Advances in natural and technological hazards research* (Vol. 31, pp. 123–132). Springer. https://doi.org/10.1007/978-94-007-2162-3_11

Yuxiang, D., Hesp, P. A., Dequan, H., & Namikas, S. L. (2017). Geomorphology Flow dynamics and sediment transport over a reversing barchan, Changli, China. *Geomorphology*, *278*, 121–127. https://doi.org/10.1016/j.geomorph.2016.11.004